Analyst

PAPER

View Article Online
View Journal

Cite this: DOI: 10.1039/d6an00189k

Fluorous nanoemulsion optodes with Förster resonance energy transfer-based fluorescence amplification toward highly-sensitive and selective detection of perfluorooctanesulfonate

Soraka Iwamoto, Tatsuro Endo and Hideaki Hisamoto *

As a fundamental study toward highly sensitive perfluorooctanesulfonate ($PFOS^-$) sensing using fluorous nanoemulsion (NE) optodes, fluorescence enhancement by Förster resonance energy transfer (FRET) was investigated. By incorporating fluoroalkyl-containing donor and acceptor dyes into hydrophobic nanodroplets, efficient FRET was realized, and the acceptor fluorescence intensity was enhanced by approximately 9.3 times compared to the conventional system without FRET. Fluorous NE optodes with FRET exhibited higher sensitivity to low $PFOS^-$ concentrations and the lowest detectable $PFOS^-$ concentration was on the order of 10^{-8} to 10^{-7} M. On the other hand, the response of interfering anions was suppressed by introducing fluoroalkyl chains into the donor dye matrix. It was revealed that the relative selectivity of $PFOS^-$ against interfering anions was improved by one to three orders of magnitude in logarithmic selectivity coefficient ($\log K^{opt}_{PFOS^-,j}$). Furthermore, the applicability of the method was further demonstrated by $PFOS^-$ detection in tap water and artificial seawater, where concentration-dependent responses were maintained under appropriate conditions.

Received 17th February 2026,
Accepted 15th May 2026

DOI: 10.1039/d6an00189k

rsc.li/analyst

Introduction

Perfluorooctane sulfonic acid (PFOS) is a representative perfluorinated organic compound that is extremely resistant to degradation and therefore persists in the environment for long periods. In addition, because it tends to bioaccumulate, PFOS has been suggested to pose serious risks to ecosystems and human health, and it has been globally regulated as a persistent environmental pollutant.[1–3] Currently, PFOS is mainly detected by liquid chromatography-mass spectrometry (LC-MS) and liquid chromatography-tandem mass spectrometry (LC-MS/MS).[4] Although these analytical techniques offer high sensitivity and specificity, they require expensive equipment and complex sample pretreatment, and are also time-consuming and unportable. Therefore, for long-term and large-scale monitoring of PFOS in the environment, the development of novel analytical methods that are simple, rapid, low-cost, and capable of on-site detection is strongly demanded.[4–7] Against this background, various optical sensing approaches based on colorimetric and fluorescence have been reported for the simple detection of PFOS.[8–19] Although these methods offer advantages such as simplicity, they often suffer from limitations in sensitivity, selectivity, or response time. Therefore, the development of a sensing platform that simultaneously achieves these requirements remains an important challenge.

On the other hand, as represented by PFOS, highly fluorinated compounds with fluoroalkyl chains are generally referred to as fluorous compounds, which are known for their unique properties. In particular, fluorous compounds exhibit strong affinity with each other while being almost immiscible with other types of molecules.[20–22] This unique property has been exploited in so-called "fluorous chemistry", which has been applied in analytical chemistry. For example, ion-selective electrodes (ISEs) incorporating fluorous membranes containing functional fluorous molecules have been reported.[23–27] In such systems, the extraction of interfering species is suppressed while ion-pair interactions are enhanced, resulting in highly selective and sensitive ion sensing.

Over the past few decades, optodes, which are optical sensors based on plasticized poly(vinyl chloride) (PVC) films, have been extensively studied. While exhibiting response mechanisms similar to those of ISEs, these sensors offer advantages such as low cost, visual detection, and miniaturization.[28–37] Our group have introduced lipophilic dye liquids as plasticizers in place of conventional ones such as bis(2-ethyhexyl) sebacate (DOS), thereby increasing the dye concentration in the film and successfully enhancing

Department of Applied Chemistry, Graduate School of Engineering, Osaka Metropolitan University, 1-1 Gakuen-cho, Naka-ku, Sakai, Osaka, 599-8531, Japan. E-mail: hisamoto@omu.ac.jp

sensitivity.[35–37] Furthermore, by introducing Förster resonance energy transfer (FRET), highly sensitive anion sensing through fluorescence enhancement was achieved, resulting in an approximately 22-fold improvement in sensitivity compared to conventional optodes.[38] However, because ion diffusion into the bulk PVC film requires a certain amount of time, the slow response speed remained a critical issue.

As a new approach to addressing these issues, nanoemulsion (NE) optodes, in which oil droplets containing hydrophobic dyes and ionophores are dispersed in water, have been developed.[32,39–42] Owing to their large specific surface area and short diffusion distance derived from nanosized droplets, NE optodes exhibit significantly faster response times than conventional film-based systems and enable rapid measurements simply by mixing with the sample solution. Our group have constructed NE optodes using lipophilic dye liquids, and have achieved highly sensitive sensing.[43–45] Furthermore, studies are underway to develop highly portable devices for on-site sensing.[46]

Therefore, we have focused on developing fluorous NE optodes aimed at achieving rapid and highly selective on-site sensing of PFOS. In our previous work, optodes components (lipophilic dyes and matrices) with fluoroalkyl chains were newly synthesized, and an absorbance-based detection method using fluorous NE optodes was reported, which operates on the principle of co-extraction of PFOS anions ($PFOS^-$) and protons (for co-extraction, see Fig. 1(a)).[47] In this system, the introduction of fluoroalkyl chains into the matrix effectively suppressed responses of interfering anions and improved the relative selectivity for $PFOS^-$. However, the lowest detectable $PFOS^-$ concentration was on the order of 10^{-7} to 10^{-6} M, and further sensitivity enhancement was required to detect $PFOS^-$ at lower concentrations.

In this study, fluorous NE optodes employing FRET were developed by using newly-synthesized functional molecules shown in Fig. 1(b) for highly sensitive and selective fluorescence sensing of $PFOS^-$. This approach extends the concept of FRET-based sensitivity enhancement established in PVC film-based optodes[26] to NE optodes, enabling rapid response as well as high sensitivity. Specifically, a fluoroalkyl-containing tetraphenylethylene derivative (R_f-11-TPE) was newly synthesized and employed both as the matrix of the nanodroplets and as the FRET donor dye. On the other hand, as the FRET acceptor dye, a fluoroalkyl-containing fluorescein derivative ([R_f-DUMBA][R_f-11-FL], see SI) was newly synthesized and used as a responsive dye for anion sensing based on co-extraction. In addition, to promote the extraction of $PFOS^-$, a fluoroalkyl-containing ion pair ([R_f-DUMBA][R_f-DBSI], see SI) was also synthesized and incorporated.

In conventional NE optodes, the matrix does not contain fluorescent dyes, and thus the sensitivity has depended solely on the responsive dye. In contrast, in the FRET-based fluorous NE optodes constructed in this study, the matrix itself was employed as a fluorescent donor dye, enabling FRET from the matrix to the responsive dye. Through energy concentration from a large number of donor dyes to a small number of acceptor dyes, the sensitivity per acceptor molecule was expected to be enhanced.

The response mechanism is based on the co-extraction of $PFOS^-$ and protons (Fig. 1(a)). When $PFOS^-$ is extracted from the aqueous phase to the organic phase owing to fluorous affinity, a proton is simultaneously co-extracted to maintain charge neutrality. As a result, the pH-responsive acceptor dye is protonated, leading to a change in its absorption spectrum and turning FRET off. Consequently, the $PFOS^-$ concentration

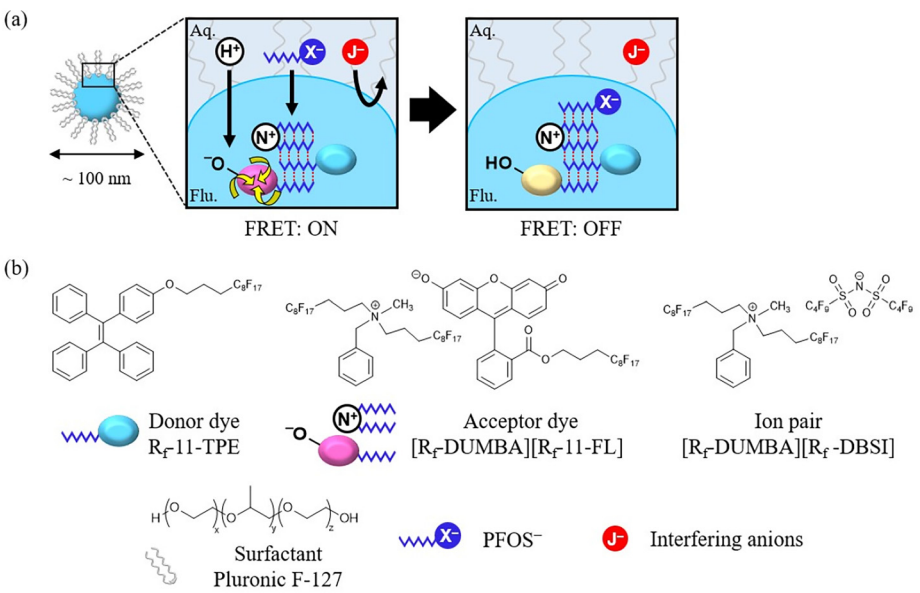

Fig. 1 (a) Illustration of FRET-based fluorous NE optodes, and schematic $PFOS^-$ sensing mechanism. (b) Chemical structure of materials for preparing NE.

can be determined from the changes in fluorescence intensity with high sensitivity and selectivity.

In this study, FRET-based fluorous NE optodes were constructed and systematically investigated for their fluorescence sensing properties of $PFOS^-$ in terms of sensitivity and selectivity. Specifically, the donor–acceptor composition was first optimized to evaluate FRET performance and its contribution to sensitivity enhancement, followed by an investigation of the response behavior toward $PFOS^-$ to elucidate the sensing mechanism of the system. Furthermore, selectivity against interfering anions was evaluated, and the applicability of the method to real samples was examined using tap water and artificial seawater.

Experimental

Reagents

Potassium perfluorooctanesulfonate (KPFOS), and perfluorooctanoic acid (PFOA) were purchased from AccuStandard Inc. (New Heaven, CT, USA). Pluronic F-127 (F-127) and trihexyltetradecylphosphonium bis(2,4,4-trimethylpentyl)phosphinate ([P_{66614}][DOP]) were purchased from Sigma-Aldrich (St. Louis, MO, USA). Sodium hydroxide (NaOH) and bis(2-ethylhexyl) sebacate (DOS) were purchased from Kanto Chemical (Tokyo, Japan). Tetrahydrofuran (THF), hydrochloric acid (HCl), 1-octanesulfonic acid sodium salt (NaOS), sodium perchlorate monohydrate ($NaClO_4 \cdot H_2O$), sodium thiocyanate (NaSCN), sodium bromide (NaBr), sodium sulfate (Na_2SO_4), oleic acid (OLA), magnesium chloride hexahydrate ($MgCl_2 \cdot 6H_2O$), calcium chloride ($CaCl_2$), and potassium chloride (KCl) were obtained from Fujifilm Wako Pure Chemical Corporation (Osaka, Japan). 2-[4-(2-Hydroxyethyl)-1-piperazinyl] ethanesulfonic acid (HEPES), and sodium chloride (NaCl) were purchased from NACALAI TESQUE, INC. (Kyoto, Japan).

Preparation and characterization of NE

The fluoroalkyl-containing donor dye, R_f-11-TPE, the fluoroalkyl-containing acceptor dye, [R_f-DUMBA][R_f-11-FL], and the fluoroalkyl-containing ion pair, [R_f-DUMBA][R_f-DBSI] were synthesized according to the prescribed procedures, as described in the SI.

NEs were prepared by adding a THF solution containing the donor dye, acceptor dye, ion pair, and surfactant (F-127) to ultrapure water, followed by sonication and removal of THF. For comparison, conventional NEs were also prepared in the same manner by using bis(2-ethyl hexyl) sebacate (DOS) instead of the donor dye and the alkyl-containing ion pair [P_{66614}][DOP] instead of the fluoroalkyl-containing ion pair. The detailed procedures and compositions are provided in the SI.

The particle size of the NEs were measured using a nanoparticle analyzer (NanoPartica SZ-100V2, HORIBA, Kyoto, Japan).

Fluorescence spectrophotometric measurements of NE

The prepared NEs were mixed with ultrapure water and HEPES buffer (pH 7.4) containing various anions ($PFOS^-$, $PFOA^-$, OS^-, ClO_4^-, SCN^-, Br^-, Cl^-, and SO_4^{2-}) or with NaOH/HCl aqueous solutions. Fluorescence spectra were measured at room temperature using a fluorescence spectrophotometer (FP-8550, JASCO CORPORATION, Tokyo, Japan). The detailed measurement conditions and sample preparation procedures are described in the figure captions and in the SI.

Evaluation in tap water and artificial seawater

The prepared NE was diluted with ultrapure water and then mixed with tap water or artificial seawater and HEPES buffer (pH 7.4) containing $PFOS^-$. Artificial seawater was prepared based on ASTM D1141 using a simplified composition consisting of major inorganic salts (NaCl, $MgCl_2$, Na_2SO_4, $CaCl_2$, and KCl). Fluorescence spectra were measured under the same conditions as described above. Detailed sample preparation conditions are provided in the figure captions and the SI.

Results and discussion

Optimization of donor–acceptor composition and FRET performance

NEs with different acceptor dye contents ([A]/[D] = 0–5.0 mol%, where A and D denote the acceptor and donor dyes, respectively) were prepared to evaluate the FRET performance and to determine the optimal acceptor dye composition. Fig. 2(a) shows the fluorescence spectra obtained under excitation at 316 nm, the absorption maximum of the donor dye. The peak at 473 nm originates from the donor dye, whereas the peak at 536 nm arises from the acceptor dye. As the acceptor content increased, the donor fluorescence intensity decreased while the acceptor fluorescence correspondingly increased, confirming that FRET occurs within the NEs.

Next, the acceptor fluorescence under FRET conditions (donor excitation) was compared with that under non-FRET conditions (direct acceptor excitation) to evaluate the fluorescence enhancement induced by FRET (Fig. 2(b)). The acceptor fluorescence intensity reached a maximum at [A]/[D] = 2.0 mol%, but decreased sharply at higher ratios. This behavior was observed regardless of the presence or absence of FRET, suggesting that concentration quenching of the acceptor dye became dominant at higher acceptor contents.

Furthermore, the FRET efficiency (FE) was calculated (Fig. S6). Although the FRET efficiency defined by the change in donor fluorescence intensity (see SI) increased monotonically with increasing acceptor content, its maximum value within the composition range (0–5.0 mol%) was only 0.67, which is lower than that reported in a previous work employing plasticized PVC films.[38] One possible reason for this is that the donor dye, R_f-11-TPE, is prone to aggregation and electrically neutral, resulting in poor affinity toward the ionic acceptor dye and spatial localization of each dye within the nanodroplets. This localization increases the average distance between the two dyes, presumably limiting the FRET efficiency.

Based on these results, [A]/[D] = 2.0 mol% was determined as the optimal composition, as it provides the highest acceptor

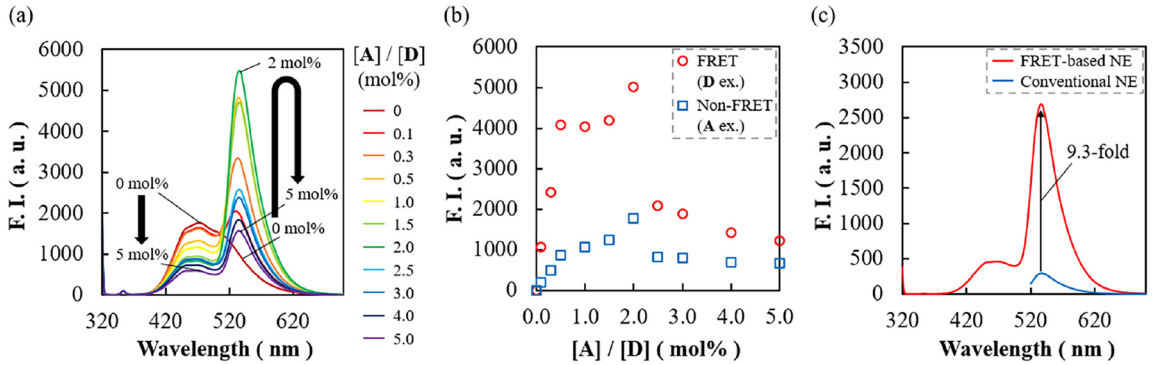

Fig. 2 (a) Fluorescence spectra of FRET-based NE with different amounts of acceptor dye added ([D] = 2.0 × 10^{-6} M, [A]/[D] = 0–5.0 mol%, λ_{ex} = 316 nm, sensitivity: medium). (b) Comparison of acceptor fluorescence intensity during FRET (donor excitation) and non-FRET (acceptor excitation) ([D] = 2.0 × 10^{-6} M, [A]/[D] = 0–5.0 mol%, λ_{ex} = 316/514 nm, λ_{em} = 536 nm, sensitivity: medium). (c) Comparison of fluorescence intensity with conventional NE ([A] = 4.0 × 10^{-7} M, λ_{ex} = 316/512 nm, λ_{em} = 536/538 nm, sensitivity: low).

fluorescence with minimal concentration quenching while also exhibiting a reasonably high FRET efficiency (>0.50). At this composition, the fluorescence enhancement factor was 2.8 and the FRET efficiency was 0.53.

To further assess the contribution of FRET to sensitivity enhancement, the FRET-based NE was compared with a conventional NE that does not employ FRET (using DOS as the matrix). As shown in Fig. 2(c), at the same acceptor dye concentration (4.0 × 10^{-7} M), the FRET-based NE exhibited a 9.3-fold increase in fluorescence intensity relative to the conventional NE. These results clearly demonstrate that the introduction of FRET significantly contributes to improving the sensitivity of NE optodes.

Evaluation of response to $PFOS^-$

The response to $PFOS^-$ was evaluated based on the optimized donor/acceptor ratio. Upon mixing the sample solution with the NE optodes, the fluorescence intensity changed immediately, and a rapid response to $PFOS^-$ was obtained within a few seconds. As shown in Fig. S7(a), the fluorescence intensity at the emission wavelength of the acceptor dye (536 nm) decreased with increasing $PFOS^-$ concentration. This behavior corresponds to the sensing mechanism of the optodes, in which the acceptor dye is protonated through the co-extraction of $PFOS^-$ and protons, confirming that the NE exhibits the expected behavior.

On the other hand, even in the sample without $PFOS^-$, the fluorescence intensity was significantly reduced compared to the NaOH solution. This background response is thought to be due to the acceptor dye (R_f11-FL) localized near the oil–water interface, which was protonated independently of co-extraction.

Next, the deprotonation rate (α) of acceptor dye was calculated to evaluate the $PFOS^-$ response (Fig. S7(b)). The response was observed in the $PFOS^-$ concentration range of 10^{-7} to 10^{-5} M, and the change in α was relatively gradual. This result indicates that this system responds in the reversible equilibrium mode, in contrast to our previously reported fluorous NE optodes, which responds in exhaustive mode in which $PFOS^-$ was almost completely extracted.[47] This is thought to be due to the matrix being a low-polarity donor dye, which limits the partitioning of $PFOS^-$ into the oil droplets.

To enhance the response sensitivity, the dye concentration was subsequently reduced to increase the $PFOS^-$-to-dye ratio. In contrast to the previously reported absorbance-based fluorous NE optode,[47] in which the dye concentration could not be significantly reduced due to sensitivity limitations, the FRET-based system enables measurements at lower dye concentrations owing to its fluorescence signal amplification.

Therefore, the NE was diluted 10-fold or 100-fold with respect to the previous measurement conditions, and its response to $PFOS^-$ was evaluated (Fig. S7(c)–(f)). Owing to the fluorescence enhancement achieved through FRET, sufficient fluorescence intensity was obtained even under highly diluted conditions. However, contrary to our expectation, the $PFOS^-$ response sensitivity decreased with increasing dilution, and almost no response was observed under the 100-fold dilution condition. This behavior can be attributed to the reduction in the organic phase volume of the NE upon dilution, while the extraction capability of this system was insufficient to effectively partition $PFOS^-$ into the nanodroplets. As a result, the extraction equilibrium shifted toward the aqueous phase. In addition, under highly diluted conditions, the relative contribution of acceptor dyes localized at the droplet interface increased, leading to an enhanced background response as clearly shown in the reduction of α value in Fig. S7(f).

These results indicate that, while the FRET-based NE provides a rapid fluorescence response and sufficient signal intensity, limited partitioning of $PFOS^-$ into the oil droplets restricts the sensitivity. To overcome this limitation, a fluoroalkyl-containing ion pair was introduced to enhance the extraction capability.

An ion-pair-containing NE ([IP]/[D] = 50 mol% where IP denotes the ion pair) was prepared, and its $PFOS^-$ concentration dependence and dye concentration dependence were evaluated in the same manner (Fig. 3(a), (b) and Fig. S8). As a

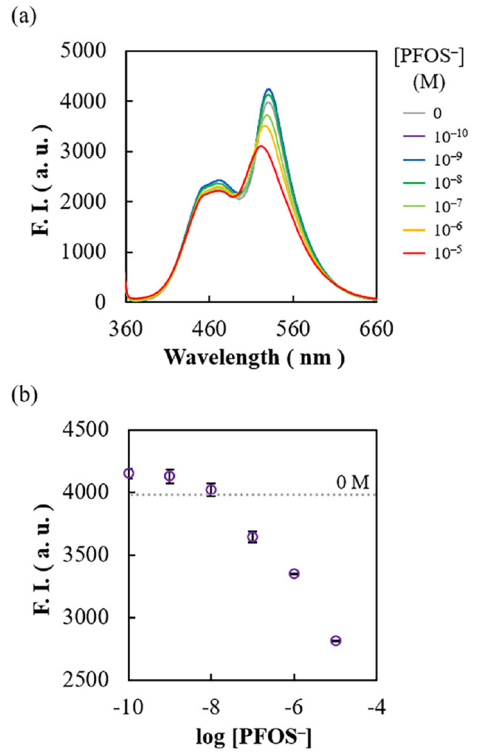

Fig. 3 (a) Fluorescence spectra for $PFOS^-$ ([D] = 2.0 × 10^{-7} M, λ_{ex} = 316 nm, sensitivity: high). (b) Response curves for $PFOS^-$ (λ_{em} = 534 nm).

result, the ion pair-containing NE showed a significant enhancement in $PFOS^-$ response sensitivity, with distinct responses observed in the low concentration range even under highly diluted conditions. The minimum detectable $PFOS^-$ concentration reached the 10^{-8} to 10^{-7} M level (Fig. 3(b)), representing approximately one order of magnitude improvement compared to the ion-pair-free FRET-based NE and our previous report.[47] This performance is comparable to, or in some cases exceeds, that of many previously reported fluorescence-based PFOS sensors. In addition, Fig. S9 shows the relationship between the change in fluorescence intensity and $PFOS^-$ concentration. Because the present system responds based on the extraction equilibrium of $PFOS^-$, no strict linear relationship was observed between the fluorescence intensity change and $PFOS^-$ concentration over a wide concentration range. In contrast, an approximately linear relationship was observed within a limited low-concentration range.

In addition, the introduction of the ion pair slightly suppressed the increase in background response under highly diluted conditions, and α was maintained within the range of approximately 0.40 to 0.50. This is likely due to enhanced ion-pair formation of the acceptor dye upon ion pair addition, thereby suppressing protonation near the interface.

These results demonstrate that the FRET-based NE system improves the detection limit for $PFOS^-$ sensing by combining the fluorescence enhancement with the control of extraction ability by adding ion pairs.

Evaluation of selectivity against interfering anions

The responses of various anions to the FRET-based NE containing ion pairs were investigated to evaluate the selectivity for $PFOS^-$ against interfering anions. To clarify the effect of the introducing fluoroalkyl chains on $PFOS^-$ selectivity, comparative experiments were performed using a conventional NE composed of non-fluorinated matrices and ion pairs.

Fig. S10 shows the response curves of various anions for the conventional NE and the FRET-based NE. Each curve was fitted using a theoretical equation based on the reversible extraction equilibrium model, and the fitted curves are shown as dashed lines. Because the FRET-based NE exhibited a relatively large background response, background correction was applied by defining the maximum response (α_{max}) as the value obtained in the buffer, taking deviations from the theoretical response into account. The selectivity coefficients, $\log K^{opt}_{PFOS^-,j}$, were then calculated from the anion concentration ratios corresponding to $\alpha = \alpha_{max}/2$ to evaluate $PFOS^-$ selectivity (Fig. 4).

Overall, the selectivity for $PFOS^-$ against interfering anions was higher for the FRET-based NE. This enhancement is attributed to the preferential extraction of $PFOS^-$ and the suppressed extraction of interfering anions induced by the fluoroalkyl chains incorporated into the oil droplet components. Compared to the conventional NE, the relative selectivity for hydrophobic organic anions ($PFOA^-$, OS^-) was improved by one order of magnitude, and the selectivity for hydrophobic inorganic anions (ClO_4^-, SCN^-) was improved by two to three orders of magnitude. Furthermore, almost no response was observed to hydrophilic inorganic anions (Br^-, Cl^-, SO_4^{2-}) even at high concentrations. The selectivity for $PFOA^-$, which has a fluoroalkyl chain similar to $PFOS^-$, was also improved.

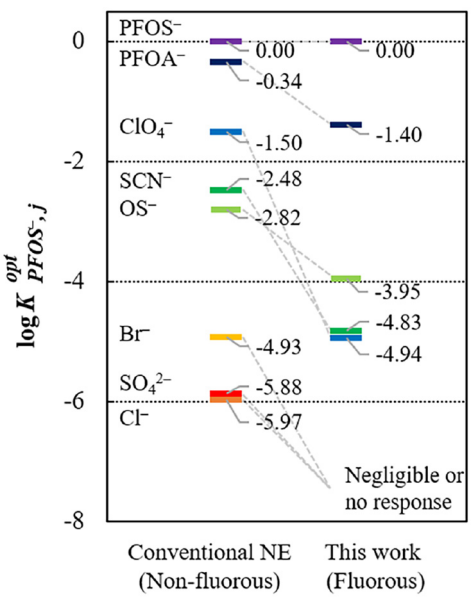

Fig. 4 Selectivity coefficients, $\log K^{opt}_{PFOS^-,j}$, of a conventional non-fluorous NE and a FRET-based fluorous NE (this work).

This is presumably because $PFOA^-$ ($C_7F_{15}COO^-$) has a shorter fluoroalkyl chain than $PFOS^-$ ($C_8F_{17}SO_3^-$), suggesting that stronger affinity is exhibited when the fluoroalkyl chain lengths are the same. These results show similar or even higher selectivity than the previously reported fluorous NE optodes,[47] indicating that the selectivity design based on the introduction of fluoroalkyl chains is effective even in the FRET-based system.

On the other hand, when high concentrations of hydrophilic inorganic anions were added, no specific response was observed, but the fluorescence intensity increased slightly (see Fig. S10(b)). Although the detailed mechanism remains unclear at present, the observed behavior may be attributed to suppression of protonation of the acceptor dye at the nanodroplet interface. In other words, high concentrations of coexisting cations may alter the protonation equilibrium of the acceptor dye, leading to a reduction in background response (protonation) and an apparent increase in fluorescence intensity. The influence of this high ionic strength-induced effect on $PFOS^-$ response was further examined in the following section using artificial seawater.

Furthermore, to evaluate the effect of superhydrophobic anions with long alkyl chains, the response to oleate anion (OLA^-: $C_{17}H_{33}COO^-$), a representative long-chain fatty acid, was investigated (Fig. S11). As a result, although the response was smaller than that for $PFOS^-$, a clear fluorescence response was observed even in the presence of OLA^-. Therefore, hydrophobic anionic compounds such as fatty acids may act as potential interfering species in this system.

These results demonstrate that the FRET-based fluorous NE optodes constructed in this study successfully achieve both enhanced sensitivity through FRET and improved $PFOS^-$ selectivity based on the incorporation of fluoroalkyl chains. On the other hand, changes in behavior under high ionic strength conditions and potential interference from long-chain hydrophobic anions such as fatty acids may occur, therefore, these effects should be taken into consideration when applying this method.

Evaluation of response to $PFOS^-$ in tap water and artificial seawater

To evaluate the practical applicability and matrix effects of the proposed method, $PFOS^-$ responses were investigated in tap water and artificial seawater. To maintain a constant pH, all samples were measured under buffered conditions.

Fig. 5 shows the $PFOS^-$ response curves obtained in buffer and in each sample matrix. In tap water, a concentration-dependent response similar to that observed in the buffer system was obtained, and the lowest detectable $PFOS^-$ concentration remained nearly unchanged at 10^{-8}–10^{-7} M. This result indicates that comparable response performance is maintained in tap water.

In contrast, in artificial seawater (original concentration: 1×), the $PFOS^-$ response sensitivity was significantly reduced, suggesting that high ionic strength suppresses the response of the system by affecting the partitioning behavior of $PFOS^-$. In addition, an overall increase in fluorescence intensity was observed, which is consistent with the changes in protonation equilibrium under high ionic strength conditions described in the previous section. However, when the artificial seawater was diluted, the response gradually recovered, and a concentration-dependent response comparable to that in the buffer system was maintained under tens-fold dilution conditions (0.05×–0.025×).

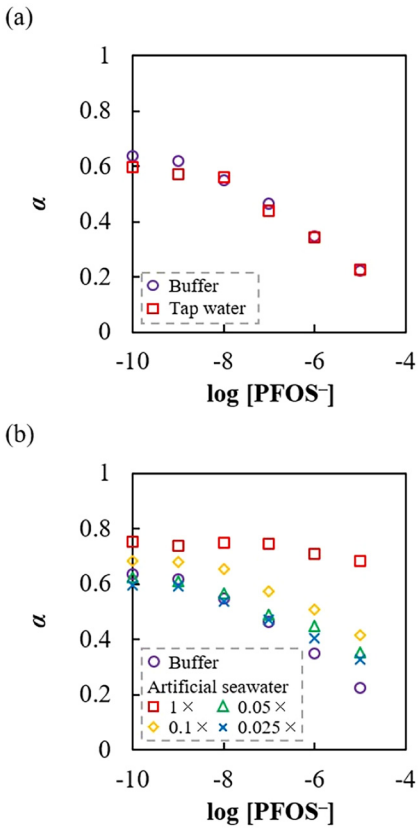

Fig. 5 Response curves for $PFOS^-$ in (a) tap water and (b) artificial seawater at different dilution conditions ([D] = 2.0×10^{-7} M, λ_{ex} = 316 nm, λ_{em} = 534 nm).

These results demonstrate that although the response of the present system is suppressed under high ionic strength conditions, it exhibits stable concentration-dependent responses toward $PFOS^-$ in relatively low to moderate ionic strength environments, including tap water. This suggests that the proposed method has practical applicability for $PFOS^-$ detection in environmental water samples.

To evaluate the sensing performance of the FRET-based fluorous NE optodes developed in this study, a comparison was made with representative previously reported PFOS detection methods in terms of detection limit (LOD), response time, and operational simplicity (Table S2).

The proposed method exhibits comparable or, in some cases, slightly higher detection limits than those of previously reported sensors, while achieving a rapid response within a few seconds simply by mixing with the sample. Many existing

PFOS sensors that achieve high sensitivity generally require a certain amount of time for signal stabilization. For example, amplifying fluorescent polymer (AFP) sensors, which exhibit extremely low detection limits (0.18 nM), require an incubation time of approximately 1 hour for target molecules to diffuse into the polymer matrix.[19] In addition, other approaches, such as those based on quantum dots[15,16] and molecularly imprinted polymers (MIPs),[17] also involve limitations including response times of several minutes (5–30 min) for signal stabilization and the need for complex pretreatment prior to measurement.

In contrast, the FRET-based fluorous NE optodes enables rapid signal generation owing to the large interfacial area of the nano-sized oil droplets, allowing for simple measurements without any pretreatment. Although the detection limit does not reach those of some highly sensitive methods, the proposed approach offers clear advantages in terms of response speed and operational simplicity. Therefore, this method is considered a promising platform for rapid $PFOS^-$ detection.

Conclusions

In this study, FRET-based fluorous NE optodes was developed for the first time, and its sensitivity and selectivity toward PFOS detection were systematically evaluated. By combining fluorescence signal amplification through FRET with enhanced ion extraction enabled by the introduction of a fluoroalkyl-containing ion pair, $PFOS^-$ was successfully detected at the 10^{-8} to 10^{-7} M level, representing an approximately one order of magnitude improvement in sensitivity compared to conventional fluorous NE optodes. Furthermore, it showed high selectivity against interfering anions, demonstrating that selectivity design based on the specific affinity between fluoroalkyl chains works effectively even in systems incorporating FRET.

The applicability of the method was further confirmed by $PFOS^-$ detection in tap water and artificial seawater, demonstrating its potential for use in realistic sample conditions. This sensor is promising as a simple and rapid on-site sensing platform, as it responds within a few seconds simply by mixing with the sample solution. Future studies should focus on optimizing the molecular design of the donor and acceptor dyes to further enhance FRET performance, ion extraction capability, and selectivity. In addition, by developing this technology into a microanalytical device, we aim to apply it to the on-site $PFOS^-$ detection in the environment.

Author contributions

S. I., T. E., and H. H. conceptualised, planned, and designed the experiments. S. I., and H. H. conceptualised the molecular designs. S. I. performed the experiments and analysed the data. S. I., T. E., and H. H. drafted the manuscript. All authors have approved the manuscript and agree with its submission to this journal.

Conflicts of interest

There are no conflicts to declare.

Data availability

All the experimental data are presented in main text and supplementary information (SI). Supplementary information is available. See DOI: https://doi.org/10.1039/d6an00189k.

Other information available upon reasonable request to corresponding author.

Acknowledgements

This study was partly supported by the Japan Society for the Promotion of Science, through a Grant-in-Aid for Scientific Research (no. 23H01990), Iketani Science and Technology Foundation and The Salt Science Research Foundation. Authors greatly acknowledge the Analytical Centre, Graduate School of Science, Osaka Metropolitan University for kind help on characterizing synthesized molecule using mass spectrometry and elemental analysis.

References

1 S. Kurwadkar, J. Dane, S. R. Kanel, M. N. Nadagouda, R. W. Cawdrey, B. Ambade, G. C. Struckhoff and R. Wilkin, *Sci. Total Environ.*, 2022, **809**, 151003.
2 E. Panieri, K. Baralic, D. Djukic-Cosic, A. B. Djordjevic and L. Saso, *Toxics*, 2022, **10**, 44.
3 J. Glüge, M. Scheringer, I. T. Cousins, J. C. Dewitt, G. Goldenman, D. Herzke, R. Lohmann, C. A. Ng, X. Trier and Z. Wang, *Environ. Sci.: Processes Impacts*, 2020, **22**, 2345–2373.
4 M. Al Amin, Z. Sobhani, Y. Liu, R. Dharmaraja, S. Chadalavada, R. Naidu, J. M. Chalker and C. Fang, *Environ. Technol. Innovation*, 2020, **19**, 100879.
5 Y. Cui, S. Wang, D. Han and H. Yan, *TrAC, Trends Anal. Chem.*, 2024, **176**, 117754.
6 S. Garg, P. Kumar, G. W. Greene, V. Mishra, D. Avisar, R. S. Sharma and L. F. Dumée, *J. Environ. Manage.*, 2022, **308**, 114655.
7 J. Zha, M. Ma, Y. Shen, L. Sun, J. Su, C. Hu, S. Wang, P. Cui, Y. Zhou and F. Liu, *Environ. Res.*, 2025, **278**, 121669.
8 C. Fang, X. Zhang, Z. Dong, L. Wang, M. Megharaj and R. Naidu, *Chemosphere*, 2018, **191**, 381–388.
9 R. F. Menger, J. J. Beck, T. Borch and C. S. Henry, *ACS ES&T Water*, 2022, **2**, 565–572.
10 H. Niu, S. Wang, Z. Zhou, Y. Ma, X. Ma and Y. Cai, *Anal. Chem.*, 2014, **86**, 4170–4177.
11 J. Liu, J. Du, Y. Su and H. Zhao, *Microchem. J.*, 2019, **149**, 104019.
12 Q. Zhang, M. Liao, K. Xiao, K. Zhuang, W. Zheng and Z. Yao, *Sens. Actuators, B*, 2022, **350**, 130851.

13 Z. Zheng, H. Yu, W.-C. Geng, X.-Y. Hu, Y.-Y. Wang, Z. Li, Y. Wang and D.-S. Guo, *Nat. Commun.*, 2019, **10**, 5762.
14 Z. Cheng, L. Du, P. Zhu, Q. Chen and K. Tan, *Spectrochim. Acta, Part A*, 2018, **201**, 281–287.
15 Z. Cheng, H. Dong, J. Liang, F. Zhang, X. Chen, L. Du and K. Tan, *Spectrochim. Acta, Part A*, 2019, **207**, 262–269.
16 F. Zhang, J. Liang, Y. Liu, Q. Zhou, Y. Hong, X. Chen and K. Tan, *Spectrochim. Acta, Part A*, 2022, **269**, 120753.
17 H. Feng, N. Wang, T. Tran, L. Yuan, J. Li and Q. Cai, *Sens. Actuators, B*, 2014, **195**, 266–273.
18 Z. Jiao, J. Li, L. Mo, J. Liang and H. Fan, *Microchim. Acta*, 2018, **185**, 473.
19 A. Concellón, J. Castro-Esteban and T. M. Swager, *J. Am. Chem. Soc.*, 2023, **145**, 11420–11430.
20 I. T. Horváth, *Acc. Chem. Res.*, 1998, **31**, 641–650.
21 R. Berger, G. Resnati, P. Metrangolo, E. Weber and J. Hulliger, *Chem. Soc. Rev.*, 2011, **40**, 3496–3508.
22 M. Cametti, B. Crousse, P. Metrangolo, R. Milani and G. Resnati, *Chem. Soc. Rev.*, 2012, **41**, 31–42.
23 P. G. Boswell and P. Bühlmann, *J. Am. Chem. Soc.*, 2005, **127**, 8958–8959.
24 P. G. Boswell, C. Szíjjártó, M. Jurisch, J. A. Gladysz, J. Rábai and P. Bühlmann, *Anal. Chem.*, 2008, **80**, 2084–2090.
25 C. Z. Lai, M. A. Fierke, R. C. da Costa, J. A. Gladysz, A. Stein and P. Bühlmann, *Anal. Chem.*, 2010, **82**, 7634–7640.
26 L. D. Chen, C. Z. Lai, L. P. Granda, M. A. Fierke, D. Mandal, A. Stein, J. A. Gladysz and P. Bühlmann, *Anal. Chem.*, 2013, **85**, 7471–7477.
27 L. D. Chen, D. Mandal, G. Pozzi, J. A. Gladysz and P. Bühlmann, *J. Am. Chem. Soc.*, 2011, **133**, 20869–20877.
28 H. Hisamoto and K. Suzuki, *Bull. Soc. Sea Water Sci., Jpn.*, 1997, **51**, 255–258.
29 E. Bakker, P. Bühlmann and E. Pretsch, *Chem. Rev.*, 1997, **97**, 3083–3132.
30 P. Bühlmann, E. Pretsch and E. Bakker, *Chem. Rev.*, 1998, **98**, 1593–1688.
31 G. Mistlberger, G. A. Crespo and E. Bakker, *Annu. Rev. Anal. Chem.*, 2014, **7**, 483–512.
32 X. Du and X. Xie, *Sens. Actuators, B*, 2021, **335**, 129368.
33 H. Hisamoto and K. Suzuki, *TrAC, Trends Anal. Chem.*, 1999, **18**, 513–524.
34 H. Hisamoto, N. Miyashita, K. Watanabe, E. Nakagawa, N. Yamamoto and K. Suzuki, *Sens. Actuators, B*, 1995, **29**, 378–385.
35 T. Mizuta, K. Sueyoshi, T. Endo and H. Hisamoto, *Sens. Actuators, B*, 2018, **258**, 1125–1130.
36 T. Mizuta, K. Sueyoshi, T. Endo and H. Hisamoto, *Bunseki Kagaku*, 2019, **68**, 945–951.
37 T. Mizuta, S. Takai, T. Nishihata, K. Sueyoshi, T. Endo and H. Hisamoto, *Analyst*, 2020, **145**, 5430–5437.
38 T. Mizuta, K. Sueyoshi, T. Endo and H. Hisamoto, *Anal. Chem.*, 2021, **93**, 4143–4148.
39 X. Xie, G. Mistlberger and E. Bakker, *Anal. Chem.*, 2013, **85**, 9932–9938.
40 X. Xie and E. Bakker, *Anal. Bioanal. Chem.*, 2015, **407**, 3899–3910.
41 X. Xie, A. Gutiérrez, V. Trofimov, I. Szilagyi, T. Soldati and E. Bakker, *Anal. Chem.*, 2015, **87**, 9954–9959.
42 L. Wang, S. Sadler, T. Cao, X. Xie, J. M. Von Filseck and E. Bakker, *Anal. Chem.*, 2019, **91**, 8973–8978.
43 R. Oishi, K. Maki, T. Mizuta, K. Sueyoshi, T. Endo and H. Hisamoto, *Analyst*, 2021, **146**, 4121–4124.
44 K. Maki, R. Oishi, T. Mizuta, K. Sueyoshi, T. Endo and H. Hisamoto, *Analyst*, 2022, **147**, 1529–1533.
45 S. Oka, K. Sueyoshi, T. Endo and H. Hisamoto, *Anal. Sci.*, 2023, **39**, 1249–1256.
46 Y. Koizumi, S. Oka, K. Sueyoshi, T. Endo and H. Hisamoto, The 27th International Conference on Miniaturized Systems for Chemistry and Life Sciences (MicroTAS), 2023, T170. f.
47 S. Iwamoto, K. Sueyoshi, T. Endo and H. Hisamoto, *Anal. Sci.*, 2024, **40**, 1787–1792.

